Progress In Electromagnetics Research Letters, Vol. 70, 129–138, 2017

Implementation of the Parallel Higher-Order FDTD with Convolution PML

Yawen Liu[1, 2, *], Pin Zhang[2], and Yiwang Chen[2]

Abstract—In this paper, a parallel Higher-order FDTD (HO-FDTD) algorithm is described. Moreover, a novel implementation of convolution PML (CPML) is presented for the HO-FDTD method. A printed microstrip patch antenna is designed to analyze the feasibility of the parallel algorithm and the absorbing performance of the CPML. Moreover, the proposed algorithm is used to deal with the large-scale computational model of the vaulted tunnel. The simulation results show that the adopted parallel strategy is feasible, and the CPML performs well in the HO-FDTD scheme.

1. INTRODUCTION

The HO-FDTD [1–12] is an efficient numerical algorithm in the time-domain. Compared with the long established FDTD method [13], HO-FDTD method shows a highly-linear dispersion performance. So with the same accuracy, larger targets can be simulated with the HO-FDTD method. However, owing to the limitation of the computer memory, the calculation can be only implemented in a finite area. So, for the intensive computation and storage, there are some challenges for its practical implementation when dealing with the electrically large and complex electromagnetic structures. To overcome the computation power and storage requirement bottlenecks, this paper focuses on the parallel implementation of the HO-FDTD$(2, 6)$. As the Message Passing Interface (MPI) [14] is becoming the new international standard for parallel programming, the MPI library is employed to exchange the electric and/or magnetic fields. For the sake of simplicity and compactness, a parallel HO-FDTD algorithm for the mode based on the one-dimension domain decomposition method is presented.

The CPML [15] is introduced to the HO-FDTD algorithm, and a planar microstrip-type structure in a 3-D case is analyzed with the parallel implementation and CPML. Furthermore, a computation model of the vaulted tunnel is established, and the impact of metallic door on the field cross-section distribution of the ultra-wideband electromagnetic pulse in the model is studied. Numerical results validate the feasibility of the parallel algorithm and the good absorbing effectiveness of the CPML.

2. PARALLEL HO-FDTD ALGORITHM

Just as the FDTD, HO-FDTD is also nearly inherently parallel in nature since only local information is needed for updating the fields at each time increment. Parallel HO-FDTD can be seen as a kind of algorithm that the whole computational domain is divided into several sub-domains, and each node only handles for the corresponding sub-domains calculation. Therefore, the requirement of computational storage and CPU time is reduced several times, which implies that the parallel HO-FDTD is faster than a serial counterpart almost by a factor n, where n is the number of processors.

Received 22 August 2017, Accepted 21 September 2017, Scheduled 2 October 2017
* Corresponding author: Yawen Liu (liuyawen1111@163.com).
[1] PLA Automobile NCO School of Army Military Transportation Institute, Bengbu 233010, China. [2] PLA Army Engineering University, Nanjing 210007, China.

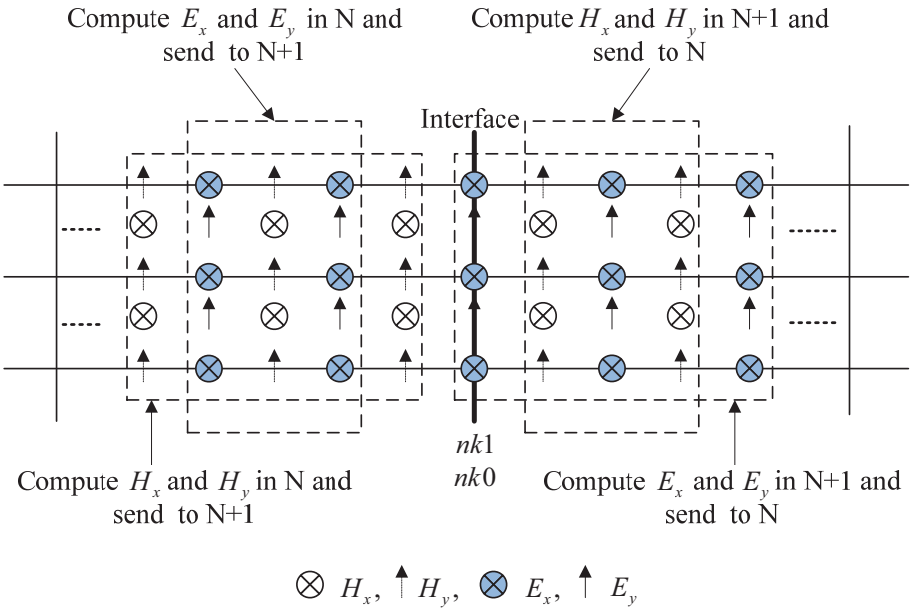

Figure 1. Two adjacent sub-domains.

The domain decomposition method (DDM) is shown in Fig. 1, and this method uses an MPI function to send the $H_{x,y}(:,:,nk1-1)$, $H_{x,y}(:,:,nk1-2)$, $H_{x,y}(:,:,nk1-3)$ and $E_{x,y}(:,:,nk1-1)$, $E_{x,y}(:,:,nk1-2)$ from the processor N to $N+1$, and to calculate the $E_{x,y}(:,:,nk0)$, $E_{x,y}(:,:,nk0+1)$, $E_{x,y}(:,:,nk0+2)$ and $H_{x,y}(:,:,nk1-1)$, $H_{x,y}(:,:,nk1-2)$ in processor $N+1$. The MPI function is once again to send the $E_{x,y}(:,:,nk0)$, $E_{x,y}(:,:,nk0+1)$, $E_{x,y}(:,:,nk0+2)$ and $H_{x,y}(:,:,nk1-1)$, $H_{x,y}(:,:,nk1-2)$ from the processor $N+1$ to N.

3. APPLICATION OF CPML TO HO-FDTD METHOD

Following the implementation procedure described in [15], the formulation in the CPML layer is posed in the stretched coordinate space. In this work, a lossy medium is assumed for the sake of generality example. The x-projection of Ampere's law is thus specified as

$$j\omega\varepsilon E_x + \sigma E_x = \frac{1}{s_y}\frac{\partial}{\partial y}H_z - \frac{1}{s_z}\frac{\partial}{\partial z}H_y, \tag{1}$$

where s_i is the stretched-coordinate metric and defined as

$$s_i = \kappa_i + \frac{\sigma_i}{\alpha_i + j\omega\varepsilon_0}, \quad i = x, y, z \tag{2}$$

where $\alpha_i > 0, \sigma_i > 0, \kappa_i \geq 1$.

Defining that $s_i' = s_i^{-1}$, we can get:

$$s' = \frac{1}{\kappa_i} + \frac{\sigma_i'}{\alpha_i' + j\omega\varepsilon_i'}, \tag{3}$$

where $\sigma_i' = -\sigma_i$, $\varepsilon_i' = \varepsilon_0\kappa_i^2$ and $\alpha_i'=\kappa_i^2\alpha_i + \kappa_i\sigma_i$. Using Laplace transform theory, it can be shown that s_i' has the impulse response

$$s_i'(t) = \frac{\delta(t)}{\kappa_i} + \frac{\sigma_i'}{\varepsilon_i'}e^{-\frac{\alpha_i'}{\varepsilon_i'}t}u(t) = \frac{\delta(t)}{\kappa_i} + \zeta_i(t) \tag{4}$$

where $\delta(t)$ is the unit impulse function and $u(t)$ the step function. Inserting Eq. (4) into Eq. (1), then transform Eq. (1) into time domain:

$$\begin{aligned}
&\varepsilon_r\varepsilon_0\frac{\partial E_x(t)}{\partial t}+\sigma E_x(t)\\
=\;& s_y'(t)*\frac{\partial}{\partial y}H_z(t)-s_z'(t)*\frac{\partial}{\partial z}H_y(t)\\
=\;&\frac{1}{\kappa_y}\frac{\partial}{\partial y}H_z(t)-\frac{1}{\kappa_z}\frac{\partial}{\partial z}H_y(t)\\
&+\int_0^t\frac{\partial}{\partial y}H_z(t-\tau)\,\zeta_y(\tau)\,d\tau-\int_0^t\frac{\partial}{\partial z}H_y(t-\tau)\,\zeta_z(\tau)\,d\tau
\end{aligned}\tag{5}$$

The discrete impulse response for $\zeta_i(t)$ can be defined as

$$S_{0_i}(m)=\int_{m\Delta t}^{(m+1)\Delta t}\zeta(\tau)d\tau=-\frac{\sigma_i}{\varepsilon_0\kappa_i^2}\int_{m\Delta t}^{(m+1)\Delta t}e^{-\left(\frac{\sigma_i}{\kappa_i\varepsilon_0}+\frac{\alpha_i}{\varepsilon_0}\right)\tau}d\tau=a_ie^{-\left(\frac{\sigma_i}{\kappa_i}+\alpha\right)_i\frac{m\Delta t}{\varepsilon_0}}\tag{6}$$

where

$$a_i=\frac{\sigma_i}{\alpha_i'}\left(e^{-\frac{\alpha_i'}{\varepsilon_i'}\Delta t}-1\right)\tag{7}$$

Then, inserting Eqs. (6) and (7) into Eq. (5), and according to the wavelet-Galerkin scheme based on Daubechies' compactly supported wavelets, the MRTD equation for E_x can be obtained as following

$$\begin{aligned}
&\varepsilon_r\varepsilon_0\frac{E^{\varphi x,n+1}_{i+\frac12,j,k}-E^{\varphi x,n}_{i+\frac12,j,k}}{\Delta t}+\sigma\frac{E^{\varphi x,n+1}_{i+\frac12,j,k}+E^{\varphi x,n}_{i+\frac12,j,k}}{2}\\
=\;&\frac{1}{\kappa_y\Delta y}\sum_l a(l)H^{\varphi z,\,n+\frac12}_{i+\frac12,j+l+\frac12,k}-\frac{1}{\kappa_z\Delta z}\sum_l a(l)H^{\varphi y,\,n+\frac12}_{i+\frac12,j,k+l+\frac12}\\
&+\frac{1}{\Delta y}\sum_{m=0}^{N-1}S_{0_y}(m)\sum_l a(l)H^{\varphi z,\,n-m+\frac12}_{i+\frac12,j+l+\frac12,k}-\frac{1}{\Delta z}\sum_{m=0}^{N-1}S_{0_z}(m)\sum_l a(l)H^{\varphi y,\,n-m+\frac12}_{i+\frac12,j,k+l+\frac12}
\end{aligned}\tag{8}$$

where $E^{\varphi x,n}_{i+\frac12,j,k}$, $H^{\varphi y,n+\frac12}_{i+\frac12,j,k+\frac12}$, and $H^{\varphi z,n+\frac12}_{i+\frac12,j+\frac12,k}$ are the coefficients for the fields and the auxiliary variables expansions in terms of scaling functions which are equal to the corresponding fields. The indexes i, j, k, and n are the discrete space and time indices related to the space and time coordinates via $x=i\Delta x$, $y=j\Delta y$, $z=k\Delta z$, and $t=n\Delta t$, where Δx, Δy, Δz, and Δt represent the space and time discretization intervals in x-, y-, z- and t-directions. Defining that

$$\psi^{n+1/2}_{e_{xy}}=\sum_{m=0}^{N-1}Z_{0_y}(m)\sum_l a(l)H^{\varphi z,n-m+\frac12}_{i+\frac12,j+l+\frac12,k}\tag{9}$$

$$\psi^{n+1/2}_{e_{xz}}=\sum_{m=0}^{N-1}S_{0_z}(m)\sum_l a(l)H^{\varphi y,\,n-m+\frac12}_{i+\frac12,j,k+l+\frac12}\tag{10}$$

Then the following equations can be easily obtained:

$$\psi^{n+1/2}_{e_{xy}}(i+1/2,j,k)=b_y\psi^{n-1/2}_{e_{xy}}(i+1/2,j,k)+\frac{a_y}{\Delta y}\sum_l a(l)H^{\varphi z,\,n-m+\frac12}_{i+\frac12,j+l+\frac12,k}\tag{11}$$

$$\psi^{n+1/2}_{e_{xz}}(i+1/2,j,k)=b_z\psi^{n-1/2}_{e_{xz}}(i+1/2,j,k)+\frac{a_z}{\Delta z}\sum_l a(l)H^{\varphi y,\,n-m+\frac12}_{i+\frac12,j,k+l+\frac12}\tag{12}$$

$$b_i=e^{-\left(\frac{\sigma_i}{\kappa_i}+\alpha_i\right)\frac{\Delta t}{\varepsilon_0}},\quad i=x,y,z\tag{13}$$

and a_i is given by Eq. (7). Then Eq. (8) can be rewritten as

$$E^{\varphi x,n+1}_{i+\frac{1}{2},j,k} = CA_m E^{\varphi x,n}_{i+\frac{1}{2},j,k} + CB_m \left[\frac{1}{\kappa_y \Delta y} \sum_l a(l) H^{\varphi z,\, n+\frac{1}{2}}_{i+\frac{1}{2},j+l+\frac{1}{2},k} - \frac{1}{\kappa_z \Delta z} \sum_l a(l) H^{\varphi y,\, n+\frac{1}{2}}_{i+\frac{1}{2},j,k+l+\frac{1}{2}} \right] + CB_m \left(\phi^{\varphi x,n+\frac{1}{2}}_{e_{xy},i+\frac{1}{2},j,k} - \phi^{\varphi x,n+\frac{1}{2}}_{e_{xz},i+\frac{1}{2},j,k} \right) \quad (14)$$

where $m = (i+\frac{1}{2}, j, k)$, and

$$CA_m = \frac{2\varepsilon_m - \sigma_m \Delta t}{2\varepsilon_m + \sigma_m \Delta t}, \quad (15)$$

$$CB_m = \frac{2\Delta t}{2\varepsilon_m + \sigma_m \Delta t} \quad (16)$$

From Eq. (14), we can see that the explicit time-marching schemes for the fields are obtained at the $(n+1)$ time step. It is obvious that the CPML implementation is independent of the material medium, and the CPML implementation requires only two auxiliary variables per field component, which is less than that reported PML and APML [16, 17]. The coefficients $a(l)$ are defined as [11]

$$a(l) = \frac{(-1)^l}{2(l+1/2)^2} \frac{[(2L-1)!!]^2}{(2L-2-2l)!!\,(2L+2l)!!} \quad (17)$$

For simplicity, here we define $L = 3$, and the coefficients for $0 \le l \le L-1$ are shown in Table 1. The coefficients $a(l)$ for $l < 0$ are given by the symmetry relation $a(-1-l) = -a(l)$.

Table 1. The coefficients $a(l)$.

l	$a(l)$
0	1.171875000
1	−0.065104167
2	0.004687500

Moreover, we use perfectly electric conductor (PEC) walls to terminate the CPML regions. Since the HO-FDTD scheme does not allow localized boundary conditions, as shown in Fig. 2, the image technique is applied to the PEC boundaries.

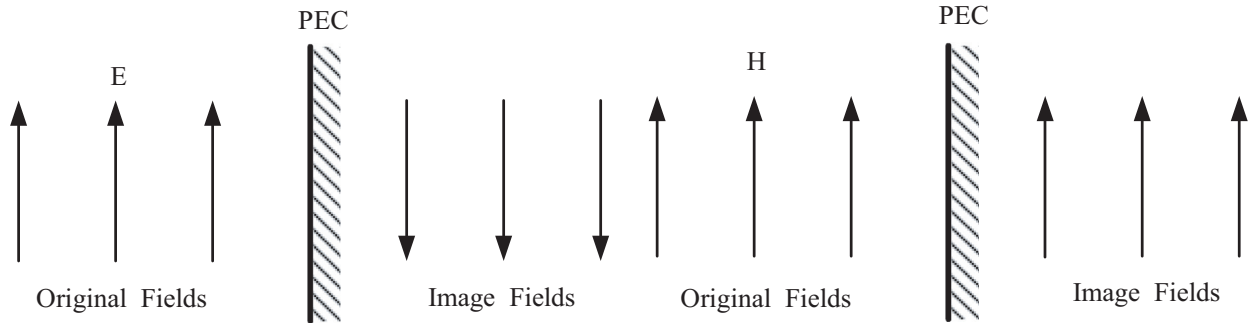

Figure 2. Original and image fields of the HO-FDTD lattice with respect to PEC boundary.

Equations for E_y and E_z are as follow:

$$E^{\varphi y,n+1}_{i,j+\frac{1}{2},k} = CA_m E^{\varphi y,n}_{i,j+\frac{1}{2},k} + CB_m \left[\frac{1}{\kappa_z \Delta z} \sum_l a(l) H^{\varphi x,\, n+\frac{1}{2}}_{i,j+\frac{1}{2},k+l+\frac{1}{2}} - \frac{1}{\kappa_x \Delta x} \sum_l a(l) H^{\varphi z,\, n+\frac{1}{2}}_{i+\frac{1}{2},j+l+\frac{1}{2},k} \right] + CB_m \left(\phi^{\varphi y,n+\frac{1}{2}}_{e_{yz},i,j+\frac{1}{2},k} - \phi^{\varphi y,n+\frac{1}{2}}_{e_{yx},i,j+\frac{1}{2},k} \right) \quad (18)$$

$$E^{\varphi z,n+1}_{i,j,k+\frac{1}{2}} = CA_m E^{\varphi z,n}_{i,j,k+\frac{1}{2}} + CB_m \left[\frac{1}{\kappa_x \Delta x} \sum_l a(l) H^{\varphi y,\, n+\frac{1}{2}}_{i+l+\frac{1}{2},j,k+\frac{1}{2}} - \frac{1}{\kappa_y \Delta y} \sum_l a(l) H^{\varphi x,\, n+\frac{1}{2}}_{i,j+l+\frac{1}{2},k+\frac{1}{2}} \right] + CB_m \left(\phi^{\varphi z,n+\frac{1}{2}}_{e_{zx},i,j,k+\frac{1}{2}} - \phi^{\varphi z,n+\frac{1}{2}}_{e_{zy},i,j,k+\frac{1}{2}} \right) \quad (19)$$

The other set of equations for updating **H** can be obtained by duality.

4. NUMERICAL RESULTS

4.1. Computation Model of the Microstrip Patch Antenna

To check whether the parallel implementation is feasible or not, comparison between serial HO-FDTD and parallel HO-FDTD is executed to analyze a printed microstrip patch antenna, whose geometry is shown in Fig. 3.

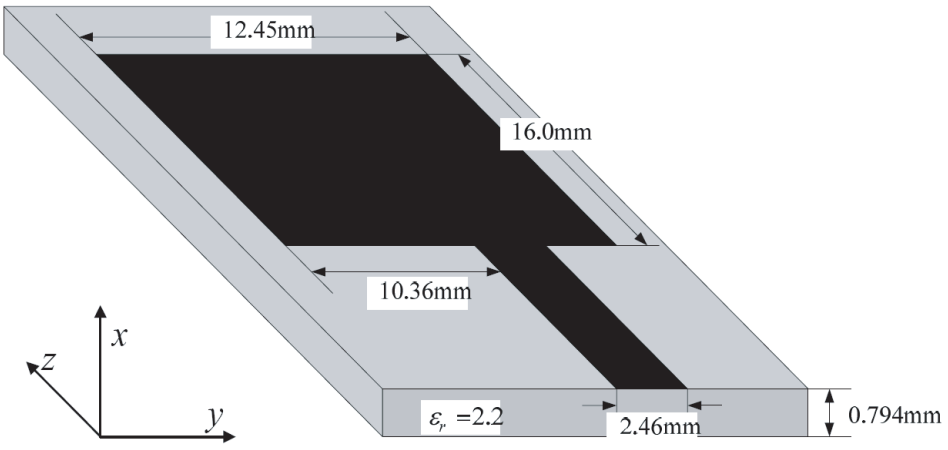

Figure 3. Geometry and dimensions of the microstrip patch antenna.

A HO-FDTD mesh of $14 \times 43 \times 62$ cells with $\Delta x = 0.265$ mm, $\Delta y = 0.83$ mm, $\Delta z = 1.0$ mm is used here. A ten-layer CPML is used to truncate both the HO-FDTD and lattices. The time discretization interval used for the HO-FDTD scheme is 0.3 ps scheme. We use the serial HO-FDTD and parallel HO-FDTD (4 PC nodes) to compute the case and then compare the S_{11} values. As shown in Fig. 4, we can conclude that parallel HO-FDTD gives the same result as serial HO-FDTD does, which validates the feasibility of the parallel HO-FDTD and the availability of the CPML. However, the serial HO-FDTD will be helpless when huge grids are involved in the computation domain, and then only parallel HO-FDTD can work.

4.2. Computation of the Vaulted Tunnel with Metallic Door

The compendious model of the tunnel and metallic door is illustrated in Fig. 5, Fig. 6 and Fig. 7(a). The tunnel is 100 m, whose dimensions are shown in Fig. 7(a). The metallic door is installed at the

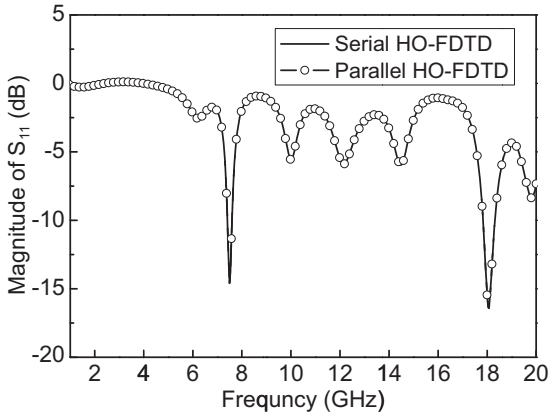

Figure 4. The magnitude of the S_{11} for the microstrip patch antenna.

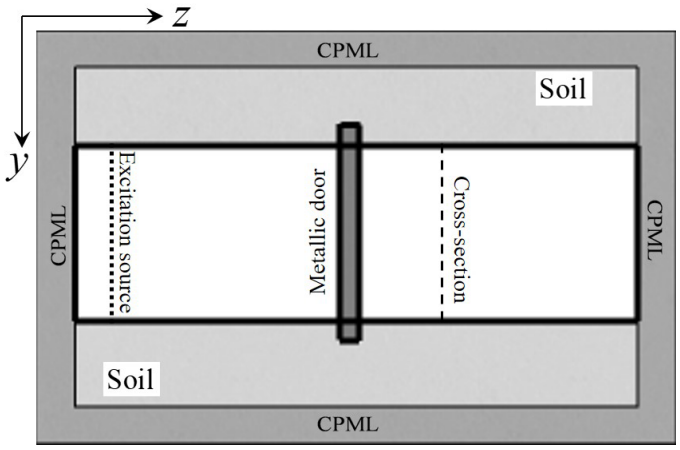

Figure 5. The computational model of the tunnel.

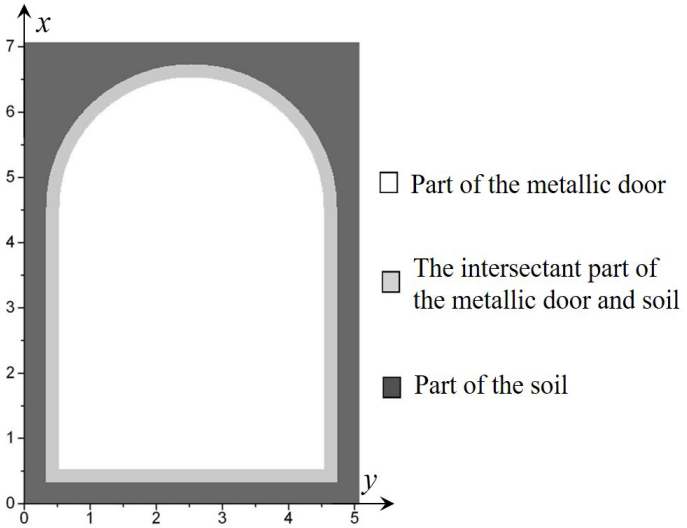

Figure 6. The computation model of the metallic door.

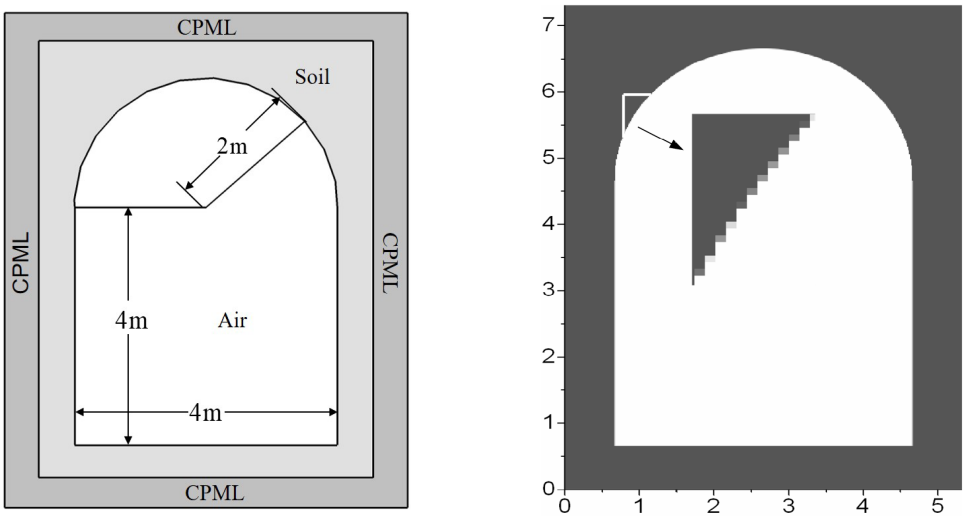

(a) (b)

Figure 7. Profile of the computation model. (a) The cross-section of the tunnel. (b) The conformed vault of the tunnel.

place of $z = 50.0\,\mathrm{m}$. The source is placed near the CPML. For the purposes of this study, constitutive parameters for soil are assumed, giving $\sigma_s = 0.004$, $\varepsilon_r = 9.0$. The constitutive parameters for the wall and arris of the straight part can be defined as $\varepsilon_{eq} = 9.0$, $\sigma_{eq} = \sigma_s/2$ and $\varepsilon_{eq} = (3\varepsilon_0\varepsilon_r + \varepsilon_0)/4$, $\sigma_{eq} = 3\sigma_s/2$.

The constitutive parameters for the wall and arris of the crooked part can be defined via the conformal technique [18]. The conformed vault of the tunnel is shown in Fig. 7(b).

In the waveguide system [13], the excitation source is usually introduced robustly according to propagation model such as TE_{10} and TM_{11}. Though in this case we cannot get the analytical model of the wave propagation, the way that the excitation sources induced in the waveguide system can still be employed here, which can be shown as follows

$$E_{\tan}^{n+1}(i,j,k_s) = E_{\tan}^{n}(i,j,k_s) + f(i,j,k_s)g(t) \tag{20}$$

where the subscript 'tan' denotes the E-field distributed in a transverse cross section at $z = k_s\Delta z$ of the tunnel structure in Fig. 5, $f(i,j,k_s)$ the function of the field distribution, and $g(t)$ the time function determining the bandwidth of the sources. Here we set $f(i,j,k_s)$ to follow the model of TM_{11} propagation in waveguide with the size of $a \times b = 4.0\,\mathrm{m} \times 6.0\,\mathrm{m}$ approximately, though the model does not satisfy the boundary condition of the tunnel, we can believe that after some length propagation, the model will be in a steady state which approaches TM_{11} propagation model of the tunnel itself.

TM_{11} propagation model is defined as

$$\left.\begin{aligned}
E_x &= -\frac{j\beta_{11}}{k_c^2}\frac{\pi}{a}A\cos\left(\frac{\pi}{a}x\right)\sin\left(\frac{\pi}{b}y\right)\ e^{-j\beta_{11}z}\\
E_y &= -\frac{j\beta_{11}}{k_c^2}\frac{\pi}{b}A\sin\left(\frac{\pi}{a}x\right)\cos\left(\frac{\pi}{b}y\right)\ e^{-j\beta_{11}z}\\
E_z &= A\sin\left(\tfrac{\pi}{a}x\right)\sin\left(\tfrac{\pi}{b}y\right)\ e^{-j\beta_{11}z}\\
H_x &= \frac{j\omega\varepsilon}{k_c^2}\frac{\pi}{b}A\sin\left(\frac{\pi}{a}x\right)\cos\left(\frac{\pi}{b}y\right)\ e^{-j\beta_{11}z}\\
H_y &= -\frac{j\omega\varepsilon}{k_c^2}\frac{\pi}{a}A\cos\left(\frac{\pi}{a}x\right)\sin\left(\frac{\pi}{b}y\right)\ e^{-j\beta_{11}z}\\
H_z &= 0
\end{aligned}\right\} \tag{21}$$

$g(t)$ in Eq. (20) is defined as a differential Gaussian electric pulse that $g(t) = E_0(t - t_0)\exp(4\pi(t-t_0)^2/\tau^2)$ with $\tau = 3.0\,\mathrm{ns}$, $E_0 = 1000\,\mathrm{V/m}$ and $t_0 = \tau$. The space is discretized with

an FDTD lattice with $\Delta x = \Delta y = \Delta z = 0.0399\,\mathrm{m}$, and ten-cell-thick PML layers terminate the grid. This results in a $170 \times 129 \times 2650$ cell lattice, and time step is $\Delta t = 57.589\,\mathrm{ps}$. $f(i, j, k_s)$ is located at the x-y plane with $z = 0.2\,\mathrm{m}$, and the sampling cross-section is located at the x-y plane with $z = 49.9867\,\mathrm{m}$ and $z = 51.0\,\mathrm{m}$. The simulation have been performed for 10000 time steps.

To get a rather efficiently absorbing ability, the parameters of CPML can be shown as

$$\begin{cases} \sigma_i = \sigma_{\max} \left(\dfrac{u - u_0}{d_{\mathrm{PML}}} \right)^m \\ \sigma_{\max} = \dfrac{m+1}{150\pi\sqrt{\varepsilon_r}\Delta s}, \quad \kappa_i = 1 + (\kappa_{\max} - 1) \left(\dfrac{|u - u_0|}{d_{\mathrm{PML}}} \right)^m \end{cases} \tag{22}$$

where $u = u_0$ is the boundary between computation domain and absorbing boundary and d_{PML} the thick of PML. In CPML, α can be set as a constant.

Figures 8(a) to 8(f) denote the cross-section distribution of the field of E_x, E_y and E_z excited by the TM_{11} propagation in the tunnel. "49.9867 m (265.0 ns)" means the filed value at the cross-section at the place of $z = 49.9867\,\mathrm{m}$ when the time step reaches 265.0 ns, and the other is analogous.

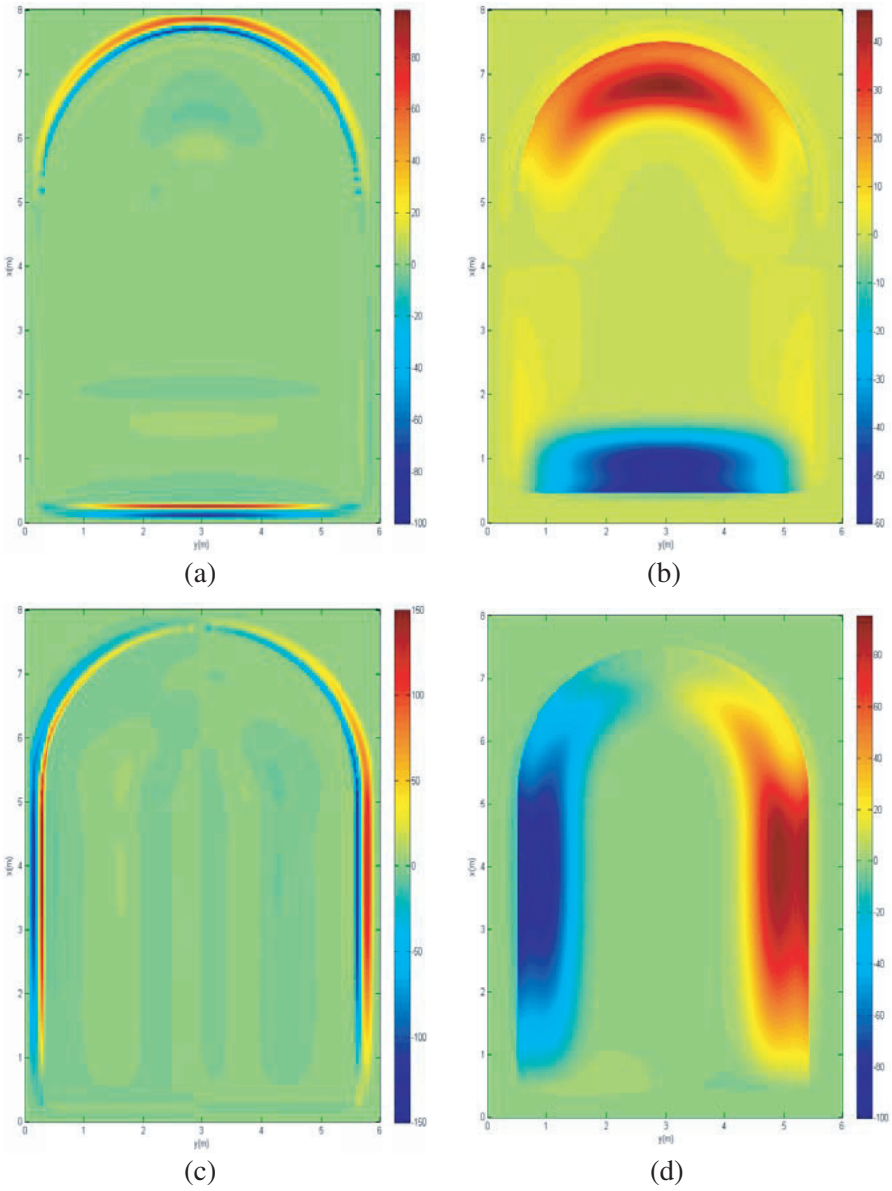

(a) (b)

(c) (d)

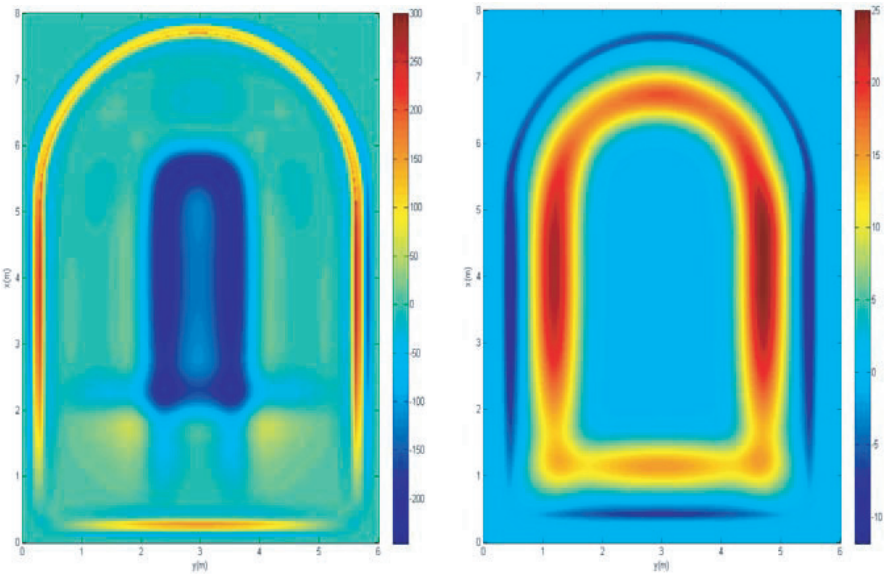

(e) (f)

Figure 8. The filed cross-section distribution. (a) E_x (V/m), 49.9867 m (265.0 ns). (b) E_x (V/m), 51.0 m (269.0 ns). (c) E_y (V/m), 49.9867 m (265.0 ns). (d) E_y (V/m), 51.0 m (269.0 ns). (e) E_z (V/m), 49.9867 m (265.0 ns). (f) E_z (V/m), 51.0 m (269.0 ns).

Observing the results, it is seen that E_x field basically distributes at the vault and the base of the tunnel, and E_y field mainly distributes at the two sides, whereas E_z field principally distributes around the tunnel. So it can be concluded how the filed gets into the space behind the metallic door: E_x field mainly circuitously propagates through the vault and the base, E_y filed through the two sides, and E_z field through circumambience of the metallic door. We can also summarize that along with the augment of the pulse propagation time, the energy of TM_{11} propagation model is centralized at the middle of the tunnel gradually.

5. CONCLUSION

In this paper, we present a parallel HO-FDTD approach. Details about the implementations of the domain decomposition, message passing between the neighboring processors are also provided, and the CPML is employed into the HO-FDTD method. It is shown that the CPML method requires only two auxiliary variables per discrete field component, which is less than that of the traditional PML and APML. Furthermore, two computation models of the microstrip patch antenna and the vaulted tunnel with metallic door are established Numerical results show that the parallel algorithm is feasible, and the CPML can provide a quite satisfactory absorbing boundary condition.

ACKNOWLEDGMENT

The authors would like to thank the reviewers for helpful remarks, and this work was supported by Natural Science Foundation of Jiangsu Province under Grant No. BK20150715.

REFERENCES

1. Young, J. L., "A higher order FDTD method for EM propagation in a collisionless cold plasma," *IEEE Trans. Antennas Propagat.*, Vol. 44, No. 9, 1283–1289, Sep. 1996.

2. Hadi, M. F. and M. Piket-May, "A modified FDTD(2, 4) scheme or modeling electrically large structures with high-phase accuracy," *IEEE Trans. Antennas Propagat.*, Vol. 45, No. 2, 254–264, Feb. 1997.
3. Teixeira, F. L. and W. C. Chew, "Lattice electromagnetic theory from a topological viewpoint," *J. Math. Phys.*, Vol. 40, No. 1, 169–187, 1999.
4. Lan, K., Y. Liu, and W. Lin, "A higher order(2, 4) scheme for reducing dispersion in FDTD algorithm," *IEEE Trans. Electromagnetic Compatibility*, Vol. 41, No. 2, 160–165, May 1999.
5. Zhang, J. and Z. Chen, "Low-dispersive super high-order FDTD schemes," *IEEE Antennas Propagat. Soc. Int. Symp.*, Vol. 3, 1510–1513, Salt Lake City, UT, Jul. 2000.
6. Hirono, T., W. Lui, S. Seki, and Y. Yoshikuni, "A three-dimensional fourth-order finite-difference time domain scheme using a symplectic integrator propagator," *IEEE Trans. Microw. Theory Tech.*, Vol. 49, No. 9, 1640–1648, Sep. 2001.
7. Prokopidis, K. P. and T. D. Tsiboukis, "Higher-order FDTD(2, 4) scheme for accurate simulations in lossy dielectrics," *Electron. Lett.*, Vol. 39, No. 11, 835–836, May 2003.
8. Shao, Z. H. and Z. X. Shen, "A generalized higher order finite-difference time-domain method and its application in guided-wave problems," *IEEE Trans. Microw. Theory Tech.*, Vol. 51, No. 3, 856–861, Mar. 2003.
9. Chun, S. T. and J. Y. Choe, "A higher order FDTD method in integral formulation," *IEEE Trans. Antennas Propagat.*, Vol. 53, No. 7, 2237–2246, Jul. 2005.
10. Wang, S., Z. Shao, and G. Wen, "A modified high order FDTD method based on wave equation," *IEEE Microwave and Wireless Components Letters*, Vol. 17, No. 5, 316–318, May 2007.
11. Chen, Y. W., Y. W. Liu, B. Chen, and P. Zhang, "A cylindrical higher order FDTD algorithm with PML and quasi PML," *IEEE Trans. Antenna Propagat.*, Vol. 61, No. 9, 4695–4704, Sept. 2013.
12. Liu, Y. W., Y. W. Chen, P. Zhang, and Z. X. Liu, "A spherical higher-order FDTD algorithm with PML," *Chinese Physics B*, Vol. 23, No. 12, 2014.
13. Taflove, A., *Computational Electrodynamics: The Finite-Difference Time-Domain Method*, Artech House, Norwood, MA, 1995.
14. Guiffaut, C. and K. Mahdjoubi, "A parallel FDTD algorithm using the MPI library," *IEEE Antennas and Propagation Magazine*, Vol. 43, 94–103, Apr. 2001.
15. Roden, J. A. and S. D. Gedney, "Convolution PML (CPML): An efficient FDTD implementation of the CFS-PML for arbitrary media," *Microwave Opt. Technol. Lett.*, Vol. 27, No. 5, 334–339, Dec. 2000.
16. Roberts, A. R. and J. Joubert, "PML absorbing boundary condition for higher-order FDTD schemes," *Electron. Lett.*, Vol. 33, No. 1, 32–34, 1997.
17. Fujii, M., M. M. Tentzeris, and P. Russer, "Performance of nonlinear dispersive APML in high-order FDTD schemes," *IEEE MTT-S International Microwave Symposium Digest*, 1129–1132, Jun. 2003.
18. Yu, W. H. and R. Mittra, "A conformal finite difference time domain technique for modeling curved dielectric surfaces," *IEEE Microwave and Wireless Components Letters*, Vol. 11, No. 1, 25–27, Jan. 2001.